Probing the surface oxidation process in hexagonal boron nitride epilayers

Cite as: AIP Advances 10, 025213 (2020); doi: 10.1063/1.5134993
Submitted: 4 November 2019 • Accepted: 29 January 2020 •
Published Online: 10 February 2020

View Online

Export Citation

CrossMark

Q. W. Wang,[a] J. Li, J. Y. Lin, 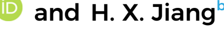 and H. X. Jiang[b]

AFFILIATIONS

Department of Electrical and Computer Engineering, Texas Tech University, Lubbock, Texas 79409, USA

[a]Author to whom correspondence should be addressed: qingwen.wang@ttu.edu
[b]Email: hx.jiang@ttu.edu

ABSTRACT

Thermal neutron detectors based on hexagonal boron nitride (*h*-BN) epilayers have demonstrated a record high efficiency among solid-state detectors at 58%. It was found that the performance of *h*-BN detectors is profoundly influenced by charge recombination at the surfaces. The dynamic process of surface oxidation in *h*-BN epilayers has been probed by x-ray photoelectron spectroscopy. The spectra of high-resolution (0.1 eV) scans indicated that the linewidth of the B 1s peak at 190.6 eV increased and the peak intensity decreased with an increase in exposure time in-air (t_{air}). The main B 1s peak at 190.6 eV evolved into multiple peaks at a higher binding energy position due to oxygen impurities tending to occupy nitrogen sites and form the B–O bond. Time constants of the oxidation process have been determined, revealing that the formation process of the B–O bond is very fast and within minutes in *h*-BN. The results suggest that reducing nitrogen vacancy generation during growth and employing surface treatment techniques would further improve the performance of *h*-BN devices.

© 2020 Author(s). All article content, except where otherwise noted, is licensed under a Creative Commons Attribution (CC BY) license (http://creativecommons.org/licenses/by/4.0/). https://doi.org/10.1063/1.5134993

Hexagonal boron nitride (*h*-BN) is a very promising ultra-wide bandgap (>6.0 eV) semiconductor with potential for many technological important applications. As the only layer-structured material among III-nitride semiconductors, *h*-BN also has potential applications in two dimensional (2D) related devices and structures, serving as an ideal template, separation and gate layer in graphene and other 2D devices.[1,2] Due to its wide bandgap, *h*-BN is a promising material for deep UV (DUV) photonic device applications[3] as well as a host for single photon emitters.[4–6] Significant progress has been made recently in the understanding of the basic properties and applications of *h*-BN through the successful synthesis of the free-standing (FS) *h*-BN epilayers with large thicknesses,[7] *h*-BN/AlGaN heterojunctions for DUV emitters,[8–10] $(BN)_{1-x}C_x$ alloys,[11,12] and *h*-$Ga_xB_{1-x}N$/BN alloys and quantum wells for possible bandgap tuning.[13,14] Most notably, ^{10}B-enriched *h*-BN (*h*-^{10}BN) epilayers have emerged as a highly promising material for solid-state neutron detector fabrication[7,15–18] and demonstrated an unprecedented high detection efficiency among all solid state neutron detectors at 58% for 1 mm^2 detectors[15] and 50% for 30 mm^2 detectors.[17] However, the detection efficiency of *h*-BN neutron detectors still falls short of the expected theoretical value because of the less than perfect charge collection efficiency, and it is shown that the surface recombination of charge carriers is one of the dominant factors, which prevents further enhancement in the charge collection efficiency in *h*-BN detectors.[16]

Like in many semiconductors, oxygen contamination could be potentially an important issue in *h*-BN device fabrication and performance. The surfaces of semiconductors can be oxidized in O_2 or air environment, generating electron/hole traps.[19] The oxidation of semiconductors can affect significantly their device performance. For example, previous studies have revealed that the photoluminescence (PL) intensity of InP is reduced when the InP surface is exposed to O_2 gas. This decrease in PL intensity after exposure to O_2 gas can be reversed by exposing InP to N_2 gas.[19] However, in GaAs, this PL intensity decrease is irreversible after exposing to O_2 gas.[19] In vertical neutron detectors fabricated from *h*-^{10}BN epilayers with two planar top and bottom electrodes, the magnitude of the effective surface recombination field is on the order of 10^4 V/cm, which impedes the charge collection and hence the overall detection efficiency and prevents further scaling up of detector size.[16] We believe that one of the causes of this large surface recombination field is *h*-BN surface oxidation in-air.

© Author(s) 2020

We report the probing of the dynamic process of oxidation on the *h*-BN surface in-air by x-ray photoelectron spectroscopy (XPS). Our results revealed that the presence of nitrogen vacancies promotes the oxidation process and oxygen impurities tend to occupy nitrogen sites. Moreover, the process of bond formation for atomic configurations related to B–O is very fast and within minutes. The results thus suggested that it is critical to reduce the nitrogen vacancy generation during epilayer growth and employ appropriate surface treatment techniques in order to further improve the performance of *h*-BN devices.

A 60 μm thick *h*-BN epilayer was grown using metal organic chemical vapor deposition (MOCVD) on the *c*-plane sapphire substrate. Trimethylboron (TMB) and ammonia (NH_3) were used as the precursors for B and N, respectively; and H_2 gas was used as a carrier gas. Due to different thermal expansion coefficients between *h*-BN and sapphire substrate, *h*-BN epilayers with a sufficient thickness will naturally separate from the sapphire substrate during the cooling process and provide freestanding (FS) *h*-BN wafers.[7,15–18] Five *h*-BN samples (A, B, C, D, and E) were prepared from the same FS *h*-BN wafer. The x-ray photoelectron spectroscopy (XPS) spectra from these *h*-BN samples were obtained from a PHI 5000 VesaProbe XPS instrument using Al Kα x rays (1486.6 eV). First, we obtained the survey scan (low resolution with 0.8 eV) spectra after the samples were cleaned using Ar ion sputtering at low voltage (500 V) to remove the oxygen and carbon contamination from the surfaces of samples. Then, four samples (B, C, D, and E) were taken out from the XPS vacuum chamber and placed in-air for different amounts of exposure times (t_{air}), ranging from 0.5 min to 60 min. Samples were then put back into the XPS vacuum chamber. The survey (low resolution with 0.8 eV) and narrow range (high resolution with 0.1 eV) scans were both measured again on all four samples after being exposed in-air with different t_{air}.

The spectra of survey scan (low resolution with 0.8 eV) from these five samples with different t_{air} are shown in Figs. 1(a)–1(e). The spectrum in Fig. 1(a) was taken from the sample A after surface sputtering as a reference sample without air exposure (t_{air} = 0 min). From samples B to E, t_{air} increased from 0.5 min to 60 min, as shown in Figs. 1(b)–1(e). Figure 1 clearly shows that the surfaces of FS *h*-BN samples absorbed carbon and oxygen impurities when exposed in-air. The results of the survey scans in Figs. 1(a)–1(e) indicate that the intensity of the O 1s peak at 532.5 eV increases significantly with t_{air} between 0 min and 60 min. The intensity of the C 1s peak at 284.8 eV also increases slightly with t_{air}. This increase in C 1s peak intensity is related to surface carbon contamination, which can be removed by Ar ion sputtering.

The high resolution (0.1 eV) spectra were obtained for all five FS *h*-BN samples (A–E), and multiple B 1s peaks were resolved with different binding energy (BE) positions, as shown in Figs. 2(a)–2(e). The spectrum in Fig. 2(a) was obtained from sample A after surface sputtering with t_{air} = 0 min. The main peak of B 1s at 190.6 eV[13] corresponds to the configuration of three N atoms bonding with one B atom in the center, as illustrated in the right inset of Fig. 2(a). The smaller peak at 189.3 eV is due to the formation of the B–C bond with one of the three N atoms replaced by one C atom and forms the B–2N–C_N configuration,[11] as illustrated in the left inset of Fig. 2(a). After exposure of sample B in air for 0.5 min, a new BE

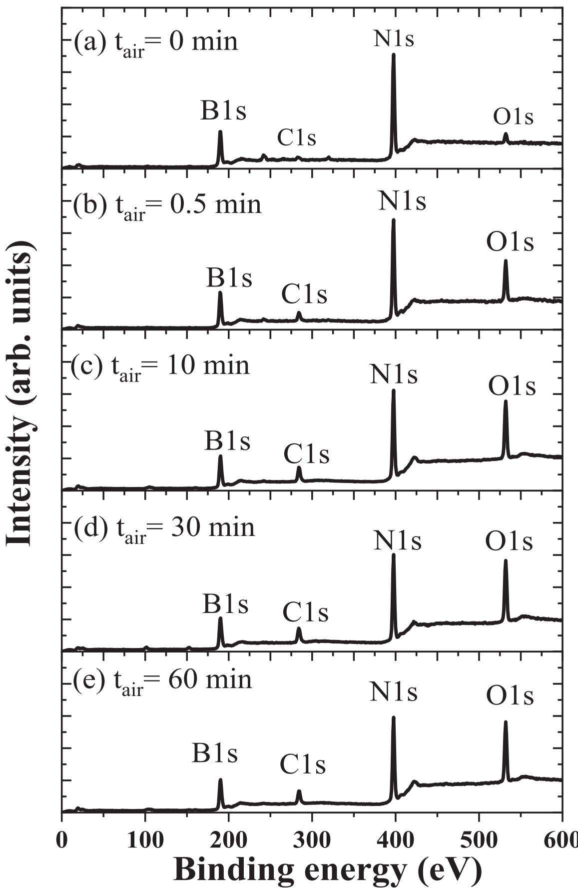

FIG. 1. XPS survey spectra with low resolution (0.8 eV) scan from five *h*-BN samples (A–E) with different air exposure times, t_{air} = (a) 0 min, (b) 0.5 min, (c) 10 min, (d) 30 min, and (e) 60 min.

peak at 192.0 eV was observed, as shown in Fig. 2(b). This peak is due to the formation of the B–O bond[20] with one O atom replacing one of the three N atoms and forming the B–2N–O_N configuration, as illustrated in the inset of Fig. 2(b). The B–O bond formation in the *h*-BN surface indicates that oxygen atoms get into *h*-BN epilayers when it is exposed in-air. This is a very quick oxidation process for the *h*-BN surface. As shown in Fig. 2(c), when t_{air} increased to 10 min for sample C, the XPS spectrum exhibited another new BE peak at 193.2 eV, which corresponds to two O atoms replacing two of three N atoms and forms the B–N–2O_N configuration, as illustrated in the inset of Fig. 2(c). The binding energy position of the B–N–2O_N configuration agrees well with that in a previous report.[21] As t_{air} further increased to 30 min and 60 min, no additional oxygen related peaks were observable in Figs. 2(d) and 2(e). However, the peak intensities of these two peaks at 192.0 eV (B–2N–O_N configuration) and 193.2 eV (B–N–2O_N configuration) clearly increased with longer exposure time, t_{air}. This indicates that more O atoms get into *h*-BN epilayers.

To further understand the B–O bond in the *h*-BN surface, we plotted the peak intensities of three different bond configurations of

© Author(s) 2020

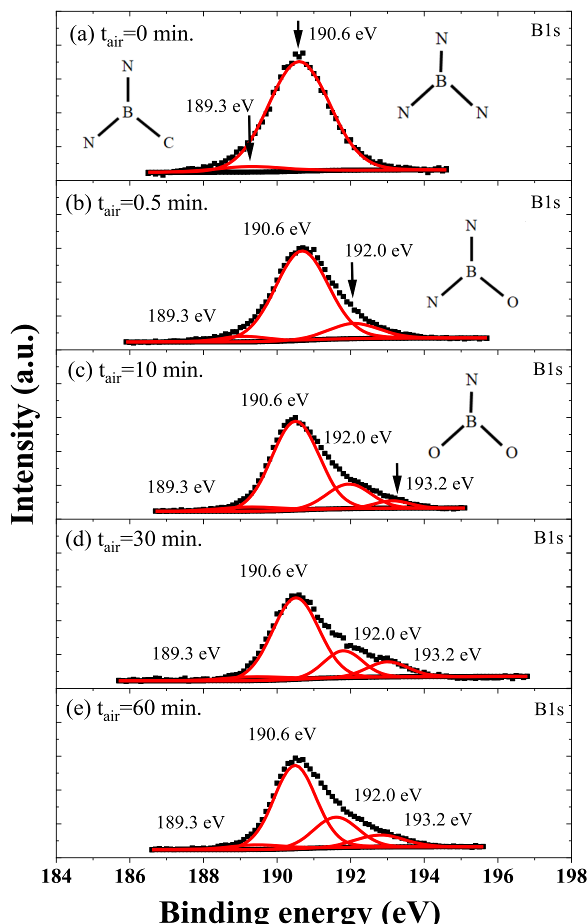

FIG. 2. XPS narrow range spectra of the B 1s peak with high resolution (0.1 eV) scan, resolving multiple peaks from five *h*-BN samples (A–E) with different air exposure times, t_{air}= (a) 0 min, (b) 0.5 min, (c) 10 min, (d) 30 min, and (e) 60 min.

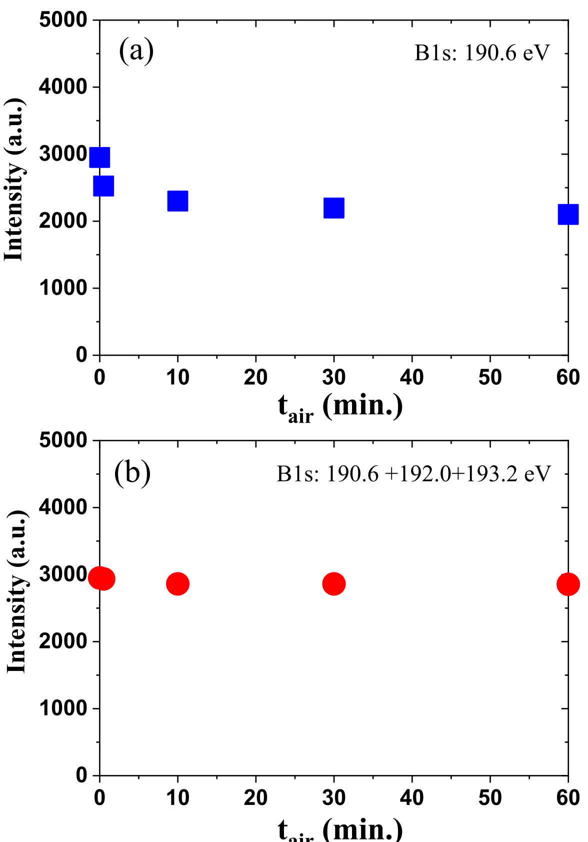

FIG. 3. (a) Total intensity of the B 1s peak at 190.6 eV of three configurations of the B atom (including B–3N, B–2N–V_N, and B–N–2V_N configurations) vs t_{air}. (b) The sum of intensities of three B 1s peaks (including B–3N at 190.6 eV, B–2N–O_N at 192.0 eV, and B–N–2O_N at 193.2 eV configurations) vs t_{air}.

the B 1s peak, including B–3N, B–2N–O_N, and B–N–2O_N, as functions of t_{air} in Fig. 3. There are three different bond states for the B 1s peak before samples exposed in-air. They are B–3N, B–2N–V_N, and B–N–2V_N, corresponding to one B atom bonding to three, two, and one N atom or equivalently with one and two N vacancies (V_N) as nearest neighbors of B atoms, respectively. The evidence for the presence of N vacancies (V_N) in *h*-BN is abundant, which are formed during the *h*-BN growth process.[22] Moreover, the Ar ion sputtering process can also generate V_N due to the bombardment of Ar ions on the *h*-BN surface, which knocks out N atoms from their original sites and produces V_N in *h*-BN epilayers.[23] It was reported that V_N is more easily to be generated than boron vacancies (V_B) with Ar ion bombardment.[24,25] However, these three configurations of the B atom have the same binding energy (BE) position at 190.6 eV in the XPS spectra. After being exposed in-air, O atoms tend to occupy these V_N sites to transform B–2N–V_N and B–N–2V_N configurations into B–2N–O_N and B–N–2O_N configurations at BE peak positions of 192.0 eV and 193.2 eV, respectively. As shown in Fig. 3(a), the total intensity of the B 1s peak at 190.6 eV of three configurations of the B atom, including B–3N, B–2N–V_N, and B–N–2V_N, decreases as t_{air} increases with most of the decrease happening in the initial time, which suggests that a fast process is involved. This is expected since the B–2N–V_N (B–N–2V_N) configuration changes into the B–2N–O_N (B–N–2O_N) configuration. However, the sum of intensities of three peaks of B–3N (190.6 eV), B–2N–O_N (192.0 eV), and B–N–2O_N (193.2 eV) is almost constant with t_{air}, as shown in Fig. 3(b). This clearly indicates again that the B–2N–O_N (B–N–2O_N) configuration is transformed from the B–2N–V_N (B–N–2V_N) configuration when *h*-BN epilayers are exposed in-air.

Figure 4(a) plots the XPS intensity (solid triangle) at 192.0 eV as a function of t_{air}. It clearly shows two different processes with an initial fast one (t_{air} < 3 min) and a slow one for longer t_{air}. The results suggested that these two processes are due to two different initial configurations for one O atom occupying one V_N site with two different time constants. The first process with a fast time constant τ_1 corresponds to one O atom getting into one of two V_N sites in the B–N–2V_N configuration and forming an intermediate configuration of B–N–O_N–V_N with a BE peak position at 192.0 eV, as illustrated in the first process of Fig. 5(a). The second process with a slow time constant τ_2 corresponds to one O atom getting into the V_N site in

© Author(s) 2020

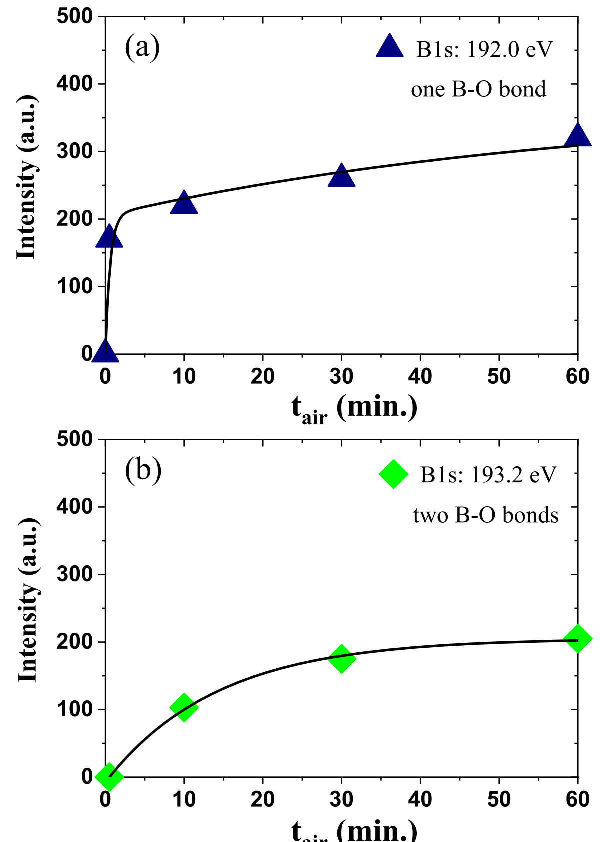

FIG. 4. (a) The XPS intensity (solid triangles) at 192.0 eV of one B–O bond and (b) intensity (solid diamonds) at 193.2 eV of two B–O bonds as functions of t_{air}. The solid curves are the least squares fits of data with Eq. (1) for (a) and Eq. (2) for (b).

the B–2N–V_N configuration and forming the B–2N–O_N configuration (192.0 eV), as illustrated in Fig. 5(b). It is obvious that one O atom getting into one of two V_N sites in the B–N–2V_N configuration is faster than one O atom getting into one V_N site in the B–2N–V_N configuration due to the higher probability of two available V_N sites in the B–N–2V_N configuration. To determine these two time constants τ_1 and τ_2, the measured XPS intensity at 192.0 eV as a function of t_{air} was fitted by the following equation:

$$I(t) = A_1 * \left(1 - e^{-\frac{t}{\tau_1}}\right) + A_2 * \left(1 - e^{-\frac{t}{\tau_2}}\right), \quad (1)$$

where A_1 and A_2 are two constants. The least squares fit of data with Eq. (1) yielded A_1 = 208 and τ_1 = 0.6 min, and A_2 = 162 and τ_2 = 60.5 min. These results suggest that the dynamic process of one O atom getting into one of two V_N sites in the B–N–2V_N configuration is much faster than that of one O atom getting into the V_N site in the B–2N–V_N configuration. The initial percentage of the B–N–2V_N (B–2N–V_N) configuration is 208/(208 + 162) = 56% (44%) after Ar ion sputtering.

The XPS intensity (solid diamond) of the B–N–2O_N configuration at 193.2 eV as a function of t_{air} is plotted in Fig. 4(b). This B–N–2O_N configuration was only observed after 0.5 min exposure in-air (t_{air} > 0.5 min). This process has only one time constant τ_3. Equation (2) is used to determine τ_3 by fitting the measured XPS intensity at 193.2 eV,

$$I(t) = B * \left(1 - e^{-\frac{t-0.5}{\tau_3}}\right) (t \geq 0.5 \text{ min}). \quad (2)$$

The least squares fit of data with Eq. (2) yielded B = 206 and τ_3 = 14.3 min. We would like to point out that the fitted value of B and A_1 is almost the same. This agrees with our explanation that B–N–O_N–V_N is an intermediate configuration evolved from the B–N–2V_N configuration and further evolves into the B–N–2O_N configuration, as shown in the second step of Fig. 5(a).

In summary, the oxidation process on the freestanding *h*-BN epilayer surface has been probed by x-ray photoelectron spectroscopy. The results indicated that three different configurations of the B–O bond are formed during the oxidation process, including two final configurations of B–2N–O_N (192.0 eV) and B–N–2O_N (193.2 eV) as well as one intermediate configuration of B–N–O_N–V_N (192.0 eV) with three different oxidation time constants of τ_1 (=0.6 min), τ_2 (=60.5 min), and τ_3(=14.3 min), respectively. Our results indicate that freestanding *h*-BN surface oxidation is a fast process within minutes. More importantly, these studies suggest

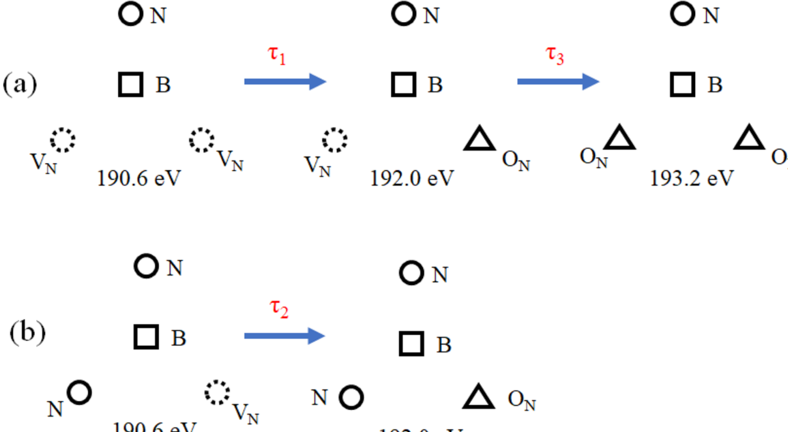

FIG. 5. Schematic diagrams illustrating the atomic configurations of two different *h*-BN surface oxidation processes: evolution (a) from the initial B–N–2V_N configuration to an intermediate configuration of B–N–O_N–V_N and to the final B–N–2O_N configuration with time constants τ_1 and τ_3 and (b) from the initial B–2N–V_N configuration to the final B–2N–O_N with a time constant τ_2.

© Author(s) 2020

that the *h*-BN device fabrication process should avoid exposure in-air and appropriate surface passivation is expected to be helpful in reducing the surface recombination field. Furthermore, reducing nitrogen vacancy point defects can also reduce the incorporation of O atoms into *h*-BN, which requires further optimization in the MOCVD growth processes.

This work was supported by DOE ARPA-E (Grant No. DE-AR000964). The DOE NNSA SSAA program (Grant No. DE-NA0002927) supported the initial *h*-BN materials growth and detector development efforts. H. X. Jiang and J. Y. Lin are grateful to the AT&T Foundation for the support of Ed Whitacre and Linda Whitacre endowed chairs.

REFERENCES

[1] C. R. Dean, A. F. Young, I. Meric, C. Lee, L. Wang, S. Sorgenfrei, K. Watanabe, T. Taniguchi, P. Kim, K. L. Shepard, and J. Hone, Nat. Nanotechnol. **5**, 722 (2010).
[2] A. K. Geim and I. V. Grigorieva, Nature **499**, 419 (2013).
[3] K. Watanabe, T. Taniguchi, and H. Kanda, Nat. Mater. **3**, 404 (2004).
[4] T. T. Tran, C. Elbadawi *et al.*, ACS Nano **10**, 7331 (2016).
[5] T. T. Tran, K. Bray, M. J. Ford *et al.*, Nat. Nanotechnol. **11**, 37 (2016).
[6] R. bourrellier, S. Meuret *et al.*, Nano Lett. **16**, 4317 (2016).
[7] A. Maity, T. C. Doan, J. Li, J. Y. Lin, and H. X. Jiang, Appl. Phys. Lett. **109**, 072101 (2016).
[8] R. Dahal, J. Li, S. Majety, B. N. Pantha, X. K. Cao, J. Y. Lin, and H. X. Jiang, Appl. Phys. Lett. **98**, 211110 (2011).
[9] S. Majety, J. Li, X. K. Cao, R. Dahal, B. N. Pantha, J. Y. Lin, and H. X. Jiang, Appl. Phys. Lett. **100**, 061121 (2012).
[10] D. A. Laleyan, S. Zhao, S. Y. Woo, H. N. Tran, H. B. Le, T. Szkopek, H. Guo, G. A. Botton, and Z. Mi, Nano Lett. **17**, 3738 (2017).
[11] M. R. Uddin, S. Majety, J. Li, J. Y. Lin, and H. X. Jiang, J. Appl. Phys. **115**, 093509 (2014).
[12] M. R. Uddin, J. Li, J. Y. Lin, and H. X. Jiang, J. Appl. Phys. **117**, 215703 (2015).
[13] Q. W. Wang, M. R. Uddin, X. Z. Du, J. Li, J. Y. Lin, and H. X. Jiang, Appl. Phys. Express **12**, 011002 (2019).
[14] Q. W. Wang, J. Li, J. Y. Lin, and H. X. Jiang, J. Appl. Phys. **125**, 205703 (2019).
[15] A. Maity, S. J. Grenadier, J. Li, J. Y. Lin, and H. X. Jiang, J. Appl. Phys. **123**, 044501 (2018).
[16] A. Maity, S. J. Grenadier, J. Li, J. Y. Lin, and H. X. Jiang, J. Appl. Phys. **125**, 104501 (2019).
[17] A. Maity, S. J. Grenadier, J. Li, J. Y. Lin, and H. X. Jiang, Appl. Phys. Lett. **114**, 222102 (2019).
[18] S. J. Grenadier, A. Maity, J. Li, J. Y. Lin, and H. X. Jiang, Appl. Phys. Lett. **112**, 162103 (2018).
[19] H. Nagai and Y. Noguchi, Appl. Phys. Lett. **33**, 312 (1978); J. Appl. Phys. **50**, 1544 (1979).
[20] D. Schild, S. Ulrich, J. Ye, and M. Stuber, Solid State Sci. **12**, 1903 (2010).
[21] M. M. Ennaceur and B. Terreault, J. Nucl. Mater. **280**, 33 (2000).
[22] X. Z. Du, J. Li, J. Y. Lin, and H. X. Jiang, Appl. Phys. Lett. **106**, 021110 (2015).
[23] R. Peter, A. Bozanic, M. Petravic, Y. Chen, L. J. Fan, and Y. W. Yang, J. Appl. Phys. **106**, 083523 (2009).
[24] A. Bozanic, M. Petravic, L. J. Fan, Y. W. Yang, and Y. Chen, Chem. Phys. Lett. **472**, 190 (2009).
[25] W. Orellana and H. Chacham, Phys. Rev. B **63**, 125205 (2001).

© Author(s) 2020